 

PACS numbers: 52.38.Kd; 52.70.Nc; 52.77.Bn
DOI: 10.1070/QE2005v035n10ABEH008964

# Effect of pulsed laser target cleaning on ionisation and acceleration of ions in a plasma produced by a femtosecond laser pulse

R.V. Volkov, A.A. Vorobiev, V.M. Gordienko, M.S. Dzhidzhoev, I.M. Lachko, B.V. Mar'in, A.B. Savel'ev, D.S. Uryupina

*Abstract*. **The impurity layer on the surface of a solid target is shown to exert a significant effect on the characteristics of the ion current of the laser plasma produced under the action of ultrahigh-intensity femtosecond radiation on the surface of this target. The application of pulsed laser cleaning gives rise to an additional high-energy component in the ion spectrum of the target material. It is shown that the ion current parameters of the laser plasma such as the average and highest ion charge, the highest ion energy of the target material, etc., can be controlled by varying the lead time of the cleaning laser radiation.**

***Keywords***: *femtosecond laser radiation, ion acceleration, hot plasma, interaction of radiation with matter*.

**1.** Parameters of the ion current from a plasma produced at the surface of a solid target under ultrahigh-intensity pulsed femtosecond laser irradiation are considerably determined by the existence of an impurity layer on the target surface [1 – 5]. This layer is formed even under conditions of high vacuum ($10^{-4} - 10^{-5}$ Torr and better) and consists of different hydrocarbon compounds and water vapour adsorbed by the surface as well as of the oxides of the parent target material [4 – 6]. In the first place, the presence of hydrocarbon and oxide impurities changes the elemental plasma composition. In particular, protons as well as carbon and oxygen ions were detected by mass spectrometric diagnostic techniques in the ion current from laser-produced plasmas even in the case when the parent target material did not initially contain the corresponding substances (H, C, O).

The presence of surface impurities changes not only the elemental composition of the ion current from laser plasmas. Experiments involving ion current detection indicate that a substantial fraction of absorbed laser pulse energy is eventually transformed into the kinetic energy of light impurity ions – protons in the first place [1 – 3]. In this case, both the energy per unit charge and the velocity gained by the ions of the parent target material, which usually possess a greater atomic weight, are significantly lower than the analogous parameters of the light impurity ions. Therefore, the leading edge of the plasma current does not contain the ions of the parent target material [4]. Meanwhile, for several applied problems it is necessary that the leading edge should be free from impurity ions and that the ions of the parent target material should be efficiently accelerated.

Different techniques may be employed to remove the impurity layer: thermal surface heating [3, 7], pulsed laser cleaning [4, 8], or ion beam surface etching [6]. In Ref. [4] we developed a technique for target surface cleaning by a nanosecond laser pulse with an energy density of 1 – 10 J cm$^{-2}$, which is ahead of the femtosecond laser pulse by no more than 1 ms. In particular, this approach ensures evaporation of not only the hydrocarbon and water layers, but of the oxide layer as well. The ion current in the above work was recorded employing an electrostatic mass spectrometer for a fixed ion energy per unit charge or by the time-of-flight technique.

In this paper, we performed a comparative study of the energy, mass, and charge spectra of the ions from the plasma produced by a $2 \times 10^{16}$ W cm$^{-2}$ femtosecond laser pulse at the clean and at unpurified silicon target surfaces. The surface was cleaned by the laser cleaning technique developed in our earlier work [4]. The effect of delay between the cleaning and femtosecond laser pulses on the ion energy and charge spectra was studied, with the delay varied from tens of picoseconds to one second. It was shown that varying this parameter permits controlling both the efficiency of silicon ion acceleration and the multiplicity of accelerated ions.

**2.** The experimental setup is schematically presented in Fig. 1. The p-polarised radiation of femtosecond laser system (*3*) ($\lambda = 616$ nm, $E = 0.5$ mJ, $\tau = 200$ fs) [9] was focused with an aberration-free objective onto the target surface at an angle of 45° to a spot of size $3 \times 4$ μm, producing the intensity $I \sim 2 \times 10^{16}$ W cm$^{-2}$. Target (*5*) was in interaction chamber (*1*). The residual gas pressure in the chamber was maintained at a level of $10^{-5}$ Torr.

In the interaction of ultrahigh-intensity femtosecond laser radiation with dense targets, of significance is the radiation contrast ratio – the ratio between the energy (intensity) of the main pulse and the prepulse energy (intensity). In our laser system, the contrast ratio is determined by the amplified spontaneous emission signal,

**R.V. Volkov, A.A. Vorobiev, M.S. Dzhidzhoev, D.S. Uryupina** Department of Physics, M.V. Lomonosov Moscow State University, Vorob'evy gory, 119992 Moscow, Russia;
**V.M. Gordienko, I.M. Lachko, A.B. Savel'ev** Department of Physics, International Laser Centre, M.V. Lomonosov Moscow State University, Vorob'evy gory, 119992 Moscow, Russia;
e-mail: ab_savelev@phys.msu.ru;
**B.V. Mar'in** D.V. Skobel'tsyn Research Institute of Nuclear Physics, M.V. Lomonosov Moscow State University, Moscow, Vorob'evy gory, 119992 Moscow, Russia

Received 11 April 2005; revision received 16 August 2005
*Kvantovaya Elektronika* **35** (10) 953 – 958 (2005)
Translated by E.N. Ragozin

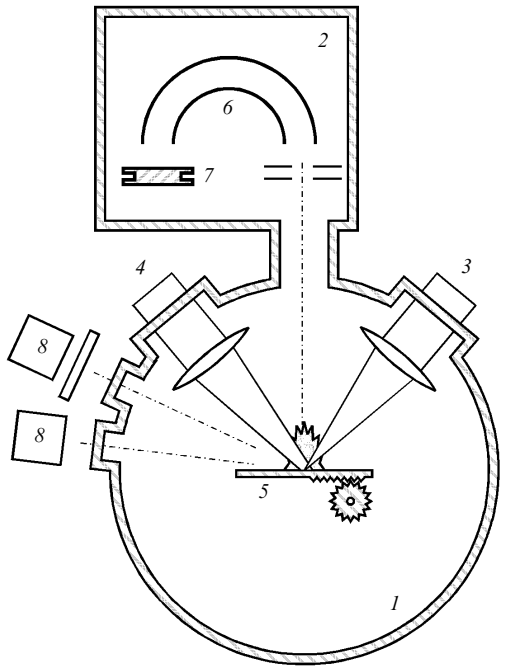


**Figure 1.** Scheme of the experimental setup: (*1*) interaction vacuum chamber; (*2*) recording vacuum chamber; (*3*) plasma-producing radiation pulse; (*4*) surface-cleaning radiation pulse; (*5*) translatable target (Si); (*6*) electrostatic mass spectrometer; (*7*) VEU-7 detector; (*8*) X-ray radiation detectors.

and the contrast ratio is controlled by introducing a saturable absorber cell into the amplification path between the second and third amplification stages [9]. An upper estimate of the spontaneous emission pulse energy $E_{ASE}$ was obtained by shuttering the femtosecond laser pulse injection into the amplifier stages.

In the absence of a saturable absorber (a small contrast ratio), $E_{ASE} \approx 50$ μJ for a femtosecond pulse energy $E \sim 500$ μJ, while in the presence of a saturable absorber (a high contrast) it was 0.5 μJ for $E \sim 300$ μJ. Measurements showed that the femtosecond radiation is focused into a spot of area $S = 9$ μm$^2$ and the radiation of spontaneous luminescence into a spot of area $S_{ASE} \approx 150 - 200$ μm$^2$ when the radiation is normally incident onto the target. Therefore, the 'effective' energy density of spontaneous emission $W_{ASE} = E_{ASE}/S_{ASE}$ does not exceed 0.3 J cm$^{-2}$ in the presence of the saturable absorber and is less than 30 J cm$^{-2}$ in its absence, while the spontaneous emission intensity $I_{ASE} = E_{ASE}/(t_{ASE}S_{ASE})$ ($\tau_{ASE} \sim 40$ ps is the duration of a spontaneous emission pulse) amounts to $\sim 10^{10}$ and $\sim 10^{12}$ W cm$^{-2}$. The intensity contrast ratio $C_I = I/I_{ASE}$ is $\sim 10^6$ and $10^4$, respectively.

It is known from the literature [10] that the ablation threshold upon irradiation of crystalline silicon by a 100-fs pulse is $\sim 0.3$ J cm$^{-2}$, this threshold rising only slightly with increasing the laser pulse duration from 100 fs to 10 ps [11]. Therefore, the spontaneous emission pulse does not evaporate the surface layer under our experimental conditions in the case of high contrast ratio. In the low-contrast case, this pulse produces a plasma layer at the target surface; prior to the arrival of the femtosecond pulse, this layer has enough time ($\sim$40 ps) to expand into vacuum to produce an electron density gradient with a characteristic scale length of 0.5–1 μm, which is roughly equal to the wavelength of the heating radiation.

Ion currents were recorded with electrostatic mass spectrometer (*6*), which was located in recording chamber (*2*), along the target normal (Fig. 1). The solid acceptance angle was equal to $8 \times 10^{-4}$ sr. The principle of operation and characteristics of the mass spectrometer are described in greater detail in Refs [5, 12]. Along with the plasma ion current, we measured the X-ray radiation yield using a two-channel analyser (comprising a photomultiplier and a NaJ scintillator) and a set of spectral filters (*8*) (Al, Be). This technique also enables estimating the average X-ray radiation energy in every experimental realisation [12, 13].

As noted above, we had earlier compared the ion currents from the laser plasmas produced at a treated target and at a target not subjected to laser cleaning [4]. The key parameters that provided the surface cleaning were the energy density $W$ of the cleaning pulse and its lead time $\Delta\tau$ relative to the femtosecond pulse. The conditions were determined for efficient laser cleaning of a titanium target. In particular, the energy density $W$ sufficient for lowering the mass impurity fraction by two orders of magnitude was equal to $\sim 0.3$ J cm$^{-2}$ and $\Delta\tau$ turned out to be bounded above by a value 1 ms: over a longer period, the impurity layer manages to partly recover due to adsorption of the residual gas contained in the vacuum chamber. On the other hand, when the time delay $\Delta\tau$ was substantially shortened, to less than several hundred nanoseconds, we observed a reduction in the total plasma current.

In our experiments, radiation beam (*4*) of an excimer XeCl laser ($\lambda = 308$ nm, $E = 10$ mJ, $\tau = 30$ ns) was injected into chamber (*1*) through its second entrance window. The radiation was focused by a lens into a spot 500 μm in diameter in the same target region as the femtosecond laser radiation. In the first series of experiments, we selected a value $\Delta\tau = 100$ μs. The delay time was subsequently varied towards longer delays (up to several seconds) and shorter delays (down to 400 ns). After every femtosecond laser pulse, the target was translated by 100 μm.

Under our experimental conditions, the target exposure to the radiation with a low contrast ratio can also be considered as the plasma production at the target surface subjected to pulsed laser treatment by its own prepulse. In this case, the lead time is $\Delta\tau = 40$ ps and $W = 30$ J cm$^{-2}$.

**3.** According to the data of X-ray plasma diagnostics, the average energy of hot electrons is $E_e = 6.5 \pm 2.2$ keV when the plasma is produced by femtosecond pulses with a high contrast ratio in the case of an unpurified target surface; for a prepurified target, $E_e = 6.6 \pm 1.8$ keV ($\Delta\tau \sim 100$ μs) and 6.0± 2.0 keV ($\Delta\tau \sim 400$ ns). No significant distinctions were observed for the absolute yield of hard X-ray plasma radiation either. Therefore, the pulsed laser cleaning had no effect on the regime of hot-electron production at the plasma–vacuum interface. When the contrast was lowered, the average energy of hot electrons slightly increased up to 7.5± 2.5 keV (unpurified target), which indicates that the role of resonance absorption of the laser energy increases in this case due to the longer gradient scale length of the plasma electron density [14].

Figure 2 shows the typical profiles of time-of-flight signals recorded with an electrostatic mass spectrometer. The analysing voltage in the spectrometer was set equal to $\sim 1.3$ kV, which ensured detecting ions with the same energy per unit ion charge ($\sim 5$ keV). In Fig. 2a, which corresponds

to the ion signal from the plasma produced by the high-contrast femtosecond radiation on an unpurified target surface, the first, and the most intense peak arises from the detection of hydrogen ions (protons) from the plasma. The remaining peaks arise from oxygen, carbon, and silicon (the parent target material) ions of different multiplicity. For a target prepurified by a nanosecond laser pulse (Figs 2b and 2c), the peaks corresponding to the detection of impurity ions vanish. A comparison of Figs 2b and 2c suggests that the length of time delay $\Delta\tau$ has a significant effect on the charge-state composition of the plasma of the parent target material. Figure 2d, which corresponds to the case when the laser plasma was produced by low-contrast femtosecond radiation, also shows some decreasing of the proton peak, which is attributable to the removal of a part of hydrocarbons by the prepulse.

To obtain the mass, charge, and energy spectra of the plasma ion current, we measured the time-of-flight mass spectrometric signals, which are analogous to those presented in Fig. 2, in the ion energy range between 400 eV and 35 keV per unit charge (for more details, see Refs [4, 5]). An analysis of mass spectra (Fig. 3) shows that the pulsed laser cleaning of the target results in a substantial suppression of the current of all impurity ions. In particular, the total fraction of hydrogen, carbon, and oxygen ions in the ion current lowers by more than an order of magnitude both for $\Delta\tau$ equal to 100 μs and to 400 ns (see Fig. 3). Making the delay $\Delta\tau$ longer than the 'optimal' value (100 μs) has the effect that the efficiency of laser treatment of the target becomes lower due to a partial recovery of the impurity layer (see also Ref. [4]).

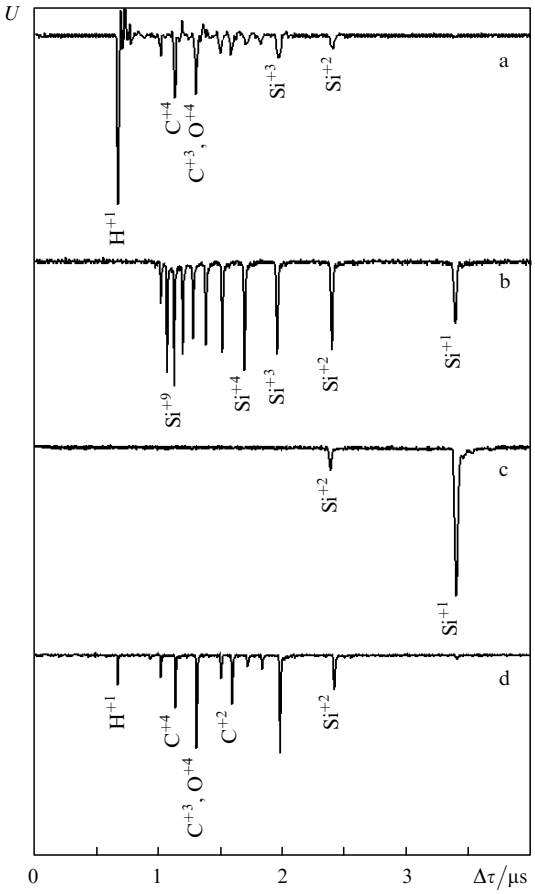


**Figure 2.** Time-of-flight signal of the plasma ions recorded with a mass spectrometer in the cases when the plasma is produced by a pulse with a high energy contrast ratio with an unpurified target (a), with a clean target for $\Delta\tau = 100$ μs (b) and 400 ns (c) as well as by a laser pulse with a low energy contrast (d) (the energy of all ions shown is ~5 keV per unit charge).

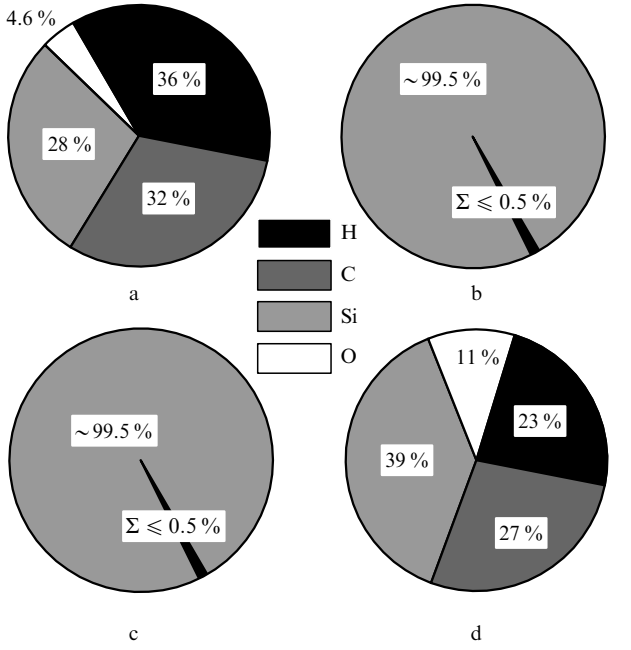


**Figure 3.** Mass spectra of the plasma ion current without application of laser treatment (a), with the use of laser cleaning for a delay $\Delta\tau = 100$ μs (b) and 400 ns (c) as well as for the radiation with a low energy contrast ratio (d).

When the target was exposed to the femtosecond radiation with a low-contrast ratio, we observed a lowering of the percentage of hydrogen and carbon ions and a growth of the content of oxygen and silicon ions. This is indication that the prepulse partly cleans the hydrocarbons from the target surface, while the oxygen, which is primarily contained in the form of silicon oxide, is not removed.

Significant changes take place also in the charge spectrum of silicon ions (Fig. 4). Removing the impurity layer from the target surface in the laser treatment with a lead time $\Delta\tau = 100$ μs gives rise to fast silicon ions with charges up to $12^+$ (Fig. 4a). This effect is attributable to the fact that the plasma front in the case of a treated surface is formed by silicon atoms, which are ionised by thermal electrons, accelerated due to hot electrons, and do not undergo recombination in their flight to the detector. Silicon atoms located at a depth in the target cannot be accelerated by hot electrons and undergo substantial recombination. This effect was comprehensively analysed in our earlier work [15].

With lengthening lead time $\Delta\tau$, the average charge of silicon ions lowers from $4^+$ to $3^+$. At the same time, the peak charge of detectable silicon ions lowers from $12^+$ to $5^+$ – a value characteristic of the initial unpurified target. Shortening the lead time $\Delta\tau$ to ~400 ns (Fig. 4b) has the effect that the average silicon ion charge falls to $1^+$ for a peak ion charge of $4^+$.

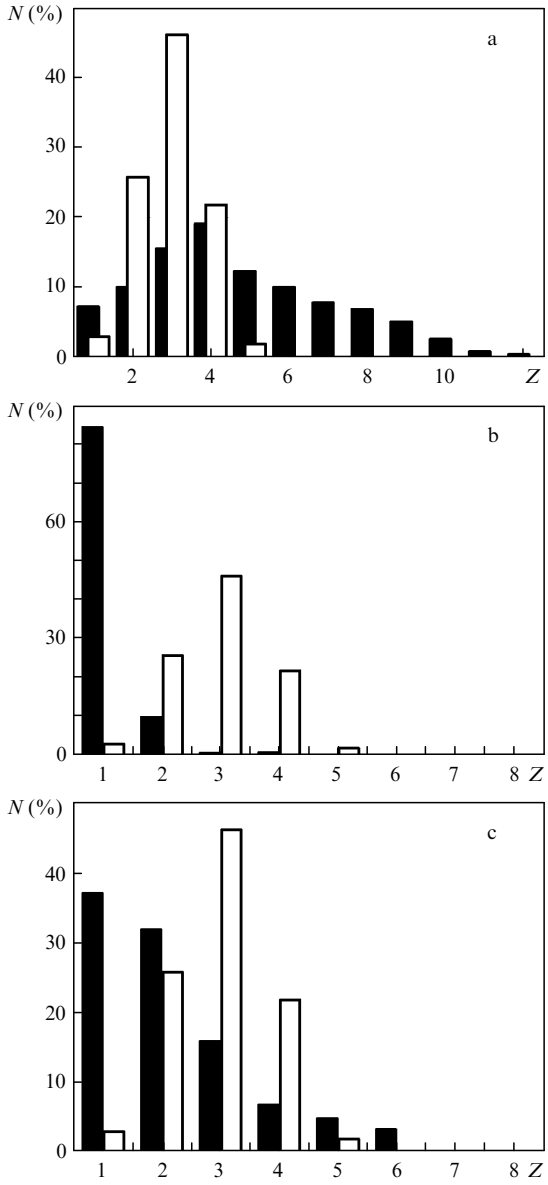


**Figure 4.** Charge spectra of silicon ions. White columns in all diagrams correspond to the charge-state distribution of Si ions in the plasma produced by a pulse with a high energy contrast with an unpurified target. The columns shown in black represent the charge-state distribution of Si ions for a laser cleaning with $\Delta\tau = 100$ μs (a) and 400 ns (b) as well as for a plasma produced by the radiation with a low energy contrast (c).

This effect is supposedly related to the dynamics of target surface cooling upon its pulsed heating. Estimates made employing a one-dimensional heat conduction equation show that during the course of a cleaning laser pulse with a duration $\tau$ and an absorbed energy density of 3 J cm$^{-2}$, a ~1-μm thick layer is heated to a temperature $T_1 > 12000\,^{\circ}$C. With neglect of the energy losses for evaporation and expansion, the time of surface cooling to a temperature $T_2 \sim 1400\,^{\circ}$C (the melting temperature of silicon) is $t_{\mathrm{cool}} \approx \tau T_2^2/T_1^2 \approx 2$ μs. Therefore, for $\Delta\tau \sim 100$ μs the surface manages to cool down completely and the evaporated material to recede from the surface by a rather long distance; for $\Delta\tau \sim 400$ ns, the surface continues to vaporise at the instant of arrival of the femtosecond radiation. Consequently, in the latter case the femtosecond radiation interacts with a strongly diffused plasma – vacuum interface rather than with a sharp boundary, and the radiation energy absorption takes place for a close-to-critical plasma density (for $\lambda = 616$ nm, $n_{\mathrm{c}} \sim 3 \times 10^{21}$ cm$^{-3}$).

The average charge also decreases significantly when low-contrast femtosecond laser radiation is used (Fig. 4c), which can also be explained by the existence of the extended electron density gradient. The differences between the spectra in Figs 4b and 4c may arise from the difference in spatial gradient scales: about 300 μm in the case of Fig. 4b and less than 1 μm in the case of Fig. 4c.

The changes in silicon ion energy spectra are most amply illustrated by the example of the silicon ion with the $2^+$ charge. Figure 5 shows the spectra obtained using a cleaned target ($\Delta\tau = 100$ μs and 400 ns) and an unpurified target, as well as the energy spectrum of the plasma ions produced by the radiation with a low energy contrast. The energy spectra for an unpurified target and a target cleaned for $\Delta\tau = 100$ μs coincide in the ion energy region $E_{\mathrm{i}} < 20$ keV. This suggests that the ionisation and acceleration processes for the silicon ions residing at some depth in the plasma, which take place due to thermal electrons, do not undergo appreciable changes. Note that the increase in the lead time to 1 s results, as would be expected, in the disappearance of the high-energy ion component of the parent material due to the recovery of the impurity layer.

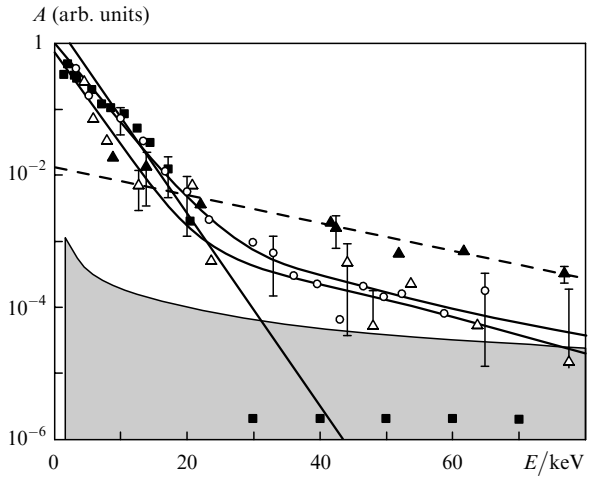


**Figure 5.** Energy spectra $A$ of the silicon ions with a charge $2^+$; ■ – uncleaned target, ○ – cleaning mode with a delay $\Delta\tau = 100$ μs, ▲ – cleaning mode with a delay $\Delta\tau = 400$ ns, △ – femtosecond laser radiation with a low energy contrast. The dashed line represents an exponential decay for 22 keV, the grey area corresponds to the noise level.

For a short lead time ($\Delta\tau = 400$ ns), we observed a significant decrease in the fraction of slow silicon ions (see Fig. 5). This behaviour may be due both to a decrease of the total ion current from the plasma in this regime [4] and to a rapid recombination of silicon ions in the extended low-density plasma.

In the ion energy range above 20 keV for an unpurified target, the signal becomes lower than the noise level, which is conventionally shown in Fig. 5. The target cleaning gives rise to fast ions with energies up to 70 keV (the highest energy which the spectrometer in use can detect for ions with the charge $2^+$). Their number for $\Delta\tau = 400$ ns is

somewhat larger than $\Delta\tau = 10$ μs. At the same time, an approximation of the energy spectrum of the $2^+$ silicon ion by an exponentially decaying function of the form $\exp(-E_i/\langle E_i\rangle)$ (here, $\langle E_i\rangle$ is the average ion energy) in the 20–70 keV ion energy range yields the same value $\langle E_i\rangle = 22 \pm 6$ keV irrespective of $\Delta\tau$. This result correlates also with X-ray diagnostic data: they suggest that the average energy of hot electrons, which determine the fast ion acceleration, remains constant (see above). The ion spectrum of the plasma produced by the radiation with a low energy contrast also contains the high-energy component.

We made a comparative analysis of the energy spectra of all ion types observed, including those for an unpurified silicon surface. The spectra of every ion were also approximated by an exponentially decaying function. For a part of the spectra of carbon ($3^+$–$6^+$) and silicon ions ($3^+$ and higher), a satisfactory result was achieved only by approximation with a sum of two exponential functions. The results shown in Fig. 6 suggest that two ion groups are present: the ions of the first group cluster near the straight line $\langle E_i\rangle = 2Z$ keV and the ions of the second group near the straight line $\langle E_i\rangle = 12Z$ keV. The first group corresponds to slow ions and the second to the fast ones. It is pertinent to note that an important part for the slow ions is played by recombination. That is why the ion charge recorded by the spectrometer is significantly different from the charge of this ion at the instant of its acceleration in the plasma. Moreover, the recombination rate also depends strongly on the ion charge. First of all, this implies that the slope (2 keV) of the straight line obtained from Fig. 6 cannot be associated with the energy of thermal electrons in the plasma. For fast ions, recombination can be neglected, and the slope of the straight line ($\alpha = 12$ keV) can be correlated with the average energy of the hot electrons as $\alpha = 2E$ [15].

The existence of two ion components both for clean and initial targets is most clearly demonstrated in Fig. 6; in this case, the fast-ion acceleration is related to hot electrons and the slow-ion acceleration to the thermal ones. The division of the ions into two components is primarily determined by their initial position relative to the target surface. The atoms located at the target surface form primarily the fast ion component, while the slow ion component is formed by the deeper located ions. In particular, when the plasma is produced at an unpurified surface, the acceleration due to hot electrons is experienced mainly by protons and partly by carbon ions. Interestingly, the fast ion component does not even contain oxygen ions, which are contained in the oxide layer on the target surface. This is indication that the ion layer accelerated by hot electrons is extremely thin. Cleaning the target surface gives rise to fast silicon ions. In the case of high-contrast femtosecond radiation, the fast component ions do not undergo recombination in their flight to the detector in vacuum. For a low contrast, even this ion group experiences substantial recombination, because the ion beam in its path encounters a cool plasma cloud ablated from the surface by the cleaning laser pulse.

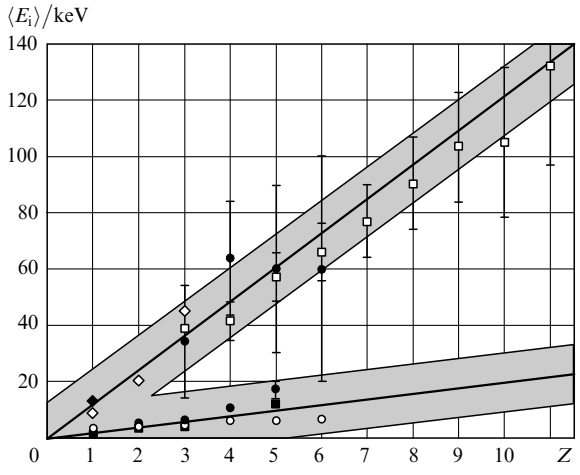


**Figure 6.** Average ion energies $\langle E_i\rangle$ as functions of $Z$ for an unpurified target (◆ – protons, ● – C, ▲ – O, ■ – Si) and a target cleaning with delays $\Delta\tau = 100$ μs (□ – high-energy Si component, ○ – low-energy Si component) and $\Delta\tau = 400$ ns (◇ – Si).

**4.** Therefore, the impurity layer exerts a significant effect on the formation of energy, elemental, and charge spectra of the ion current from the plasma of a solid target irradiated by ultrahigh-intensity femtosecond laser radiation. For the most part, the effect of impurity layer reduces to the electric screening of the ions of the parent target material from the accelerating field of hot plasma electrons. As a result, the highest energy per unit charge is acquired by the impurity ions, while the ions of the parent target material gain substantially lower velocities. The preferential acceleration of protons compared to carbon ions is evidently related to the lower $Z/M$ ratio for carbon ($M$ is the ion mass): $Z/M = 1$ for hydrogen and no greater than 0.5 for carbon.

Not only does the pulsed laser cleaning of a surface afford the production of an ion beam consisting primarily of the ions of a parent target material, but it also enables controlling the parameters of this ion beam – its energy and charge spectrum. In particular, when the cleaning pulse arrives 100 μs prior to the femtosecond one, we observed a large number of fast silicon ions with an energy of about 12 keV per unit charge and multiplicities up to $12^+$. Shortening the lead time to 400 μs lowers the charge of silicon ions to $1^+$–$2^+$ for the same energy per unit charge.

The contrast ratio of femtosecond laser radiation also exerts a significant effect on the charge and energy of accelerated ions. To obtain high-multiplicity ions requires employing femtosecond radiation with a large contrast ratio to ensure the ionisation and the ion acceleration at the sharp plasma–vacuum interface. In particular, the existence of a 40-ps prepulse with an energy density of about 30 J cm$^{-2}$ lowers the average charge of the ions detected.

To produce multiply charged heavy-ion beams by exposing the target surface to femtosecond laser radiation, the surface should be cleaned both from adsorbed and oxide layers. We believe that our findings can be extended to the case of relativistic intensities of laser radiation as well. The ion beams produced under irradiation in different regimes can be validly used in a variety of applications, including ion implantation, film deposition, production of seed beams for ion accelerators, and several other applications.

***Acknowledgements.*** This work was supported by the Russian Foundation for Basic Research (Grant No. 04-02-16341) and the ISTC (Grant No. 2651r). I.M. Lachko was supported by the INTAS (Grant No. 03-55-1982).

## References


1. Clark E.L., Krushelnuk K., Zepf M., et al. *Phys. Rev. Lett.*, **85**, 1654 (2000).
2. Badziak J., Woryna W., Parys P., et al. *Phys. Rev. Lett.*, **87**, 215001 (2001).
3. Hegelich M., Karsch S., Pretzler G., et al. *Phys. Rev. Lett.*, **89**, 85002 (2002).
4. Volkov R.V., Golishnikov D.M., Gordienko V.M., et al. *Kvantovaya Elektron.*, **33** (11), 981 (2003) [*Quantum Electron.*, **33** (11), 981 (2003)].
5. Chutko O.V., Gordienko V.M., Lachko I.M., et al. *Appl. Phys. B*, **77**, 831 (2003).
6. Allen M., Patel P.K., Mackinnon A., et al. *Phys. Rev. Lett.*, **93**, 265004 (2004).
7. Begay F., Forslund D.W. *Phys. Fluids*, **25**, 1675 (1982).
8. Dinger R., Rohr K., Weber H. *J. Phys. D: Appl. Phys.*, **17**, 1707 (1984).
9. Volkov R.V., Gordienko V.M., Dzhidzhoev M.S., et al. *Kvantovaya Elektron.*, **24**, 1114 (1997) [*Quantum Electron.*, **24**, 1081 (1997)].
10. Von der Linde D., Sokolowski-Tinten K., Bialkowski J. *Appl. Surf. Science*, **109/110**, 1 (1997).
11. Stuart B.C., Feit M.D., Herman S. *Phys. Rev. B*, **53**, 1749 (1996).
12. Gordienko V.M., Lachko I.M., Mikheev P.M., et al. *Plasma Phys. Control. Fusion*, **44**, 2555 (2002).
13. Volkov R.V., Gordienko V.M., Mikheev P.M., et al. *Kvantovaya Elektron.*, **30**, 896 (2000) [*Quantum Electron.*, **30**, 896 (2000)].
14. Gibbon P., Forster R. *Plasma Phys. Control. Fusion*, **38**, 769 (1996).
15. Gordienko V.M., Lachko I.M., Savel'ev A.B., et al. *Appl. Phys. B*, **80**, 733 (2005).